Journal of Asian Ceramic Societies 3 (2015) 266–270

Journal of Asian Ceramic Societies

journal homepage: www.elsevier.com/locate/jascer

Fabrication of ITO particles using a combination of a homogeneous precipitation method and a seeding technique and their electrical conductivity

Yoshio Kobayashi [a,*], Naomichi Takahashi [a], Takafumi Maeda [a], Takehiro Yonezawa [b], Kazuhiko Yamasaki [b]

[a] Department of Biomolecular Functional Engineering, College of Engineering, Ibaraki University, 4-12-1 Naka-narusawa-cho, Hitachi, Ibaraki 316-8511, Japan

[b] Central Research Institute, Mitsubishi Materials Corporation, 1002-14 Mukohyama, Naka, Ibaraki 311-0102, Japan

ARTICLE INFO

Article history:
Received 26 February 2015
Received in revised form 20 April 2015
Accepted 19 May 2015
Available online 9 June 2015

Keywords:
Indium tin oxide
Particles
Homogeneous precipitation method
Seeding technique
Electric conductivity

ABSTRACT

The present work proposes a method to fabricate indium tin oxide (ITO) particles using precursor particles synthesized with a combination of a homogeneous precipitation method and a seeding technique, and it also describes their electronic conductivity properties. Seed nanoparticles were produced using a co-precipitation method with aqueous solutions of indium (III) chloride, tin (IV) chloride aqueous solution and sodium hydroxide. Three types of ITO nanoparticles were fabricated. The first type was fabricated using the co-precipitation method (c-ITO). The second and third types were fabricated using a homogeneous precipitation method with the seed nanoparticles (s-ITO) and without seeds (n-ITO). The as-prepared precursor particles were annealed in air at 500 °C, and their crystal structures were cubic ITO. The c-ITO nanoparticles formed irregular-shaped agglomerates of nanoparticles. The n-ITO nanoparticles had a rectangular-parallelepiped or quasi-cubic structure. Most s-ITO nanoparticles had a quasi-cubic structure, and their size was larger than the n-ITO particles. The volume resistivities of the c-ITO, n-ITO and s-ITO powders decreased in that order because the regular-shaped particles were made to strongly contact with each other.

1. Introduction

Tin-doped indium oxide, or indium tin oxide (ITO), is the most representative among transparent electro-conductive materials used for opto-electronic devices such as displays, solar cells and sensors [1–6]. ITO films can be produced using various methods such as electron beam evaporation, PVD, sputtering, CVD and spray [5,7–15]. Although these methods are conventionally used and fundamentally and industrially studied, they have some disadvantages as follows. Because the PVD and sputtering methods are used at low pressure, their instruments require a large and costly vacuum system. For the CVD and spray methods, the as-prepared ITO films on the substrate must be annealed at high temperature during or after preparation, which thermally damages the substrate if its material is sensitive to high temperature, such as plastics.

Coating the substrate with a colloid solution that contains ITO crystalline particles is an alternative method to produce ITO films [16–18]. Because the coating method uses the crystallites, the film is not required to be annealed for crystallization. Consequently, the substrate is not thermally damaged. Methods to produce a large amount of ITO crystalline particles at low cost with low environmental load chemicals are industrially required. From this viewpoint, the methods with aqueous solution that contains inorganic salts as the main precursors, i.e., aqueous-phase methods using inorganic salts, are promising.

ITO crystalline particles can be synthesized from aqueous solutions of inorganic salts with methods such as a sol–gel method [19–23], a co-precipitation method [24–28], and a hydrothermal and solvothermal process [29,30,28], which are representative among the aqueous-phase methods. The hydrothermal and solvothermal process can be extended to production of ITO-related compounds such as InOOH and $In(OH)_3$ [31–35]. A homogeneous

* Corresponding author. Tel.: +81 294 38 5052; fax: +81 294 38 5078.
E-mail address: ykoba@mx.ibaraki.ac.jp (Y. Kobayashi).

Peer review under responsibility of The Ceramic Society of Japan and the Korean Ceramic Society.

http://dx.doi.org/10.1016/j.jascer.2015.05.006

precipitation method is an alternative method as the aqueous-phase method. In the homogeneous precipitation method, precipitators such as urea are decomposed at high temperature, which slowly and homogeneously increase the solution pH. As a result, fine metal compound nanoparticles are produced. The precipitation method using the thermal decomposition of precipitator like the homogeneous precipitation process in an aqueous solution with dissolved indium salt and tin salt can be used for fabricating ITO crystalline particles [36,37]. The homogeneous precipitation method has an advantage over the other methods. Because the particles are homogeneously produced in the solution due to the thermal decomposition of precipitator, they are mono-dispersed, which indicates that all particles should have almost identical properties. Therefore, ITO films composed of the ITO crystalline particles that are fabricated using the homogeneous precipitation method may have reliable electric conductivity.

Our research group have studied the effects of nanocrystallite seeding on various oxides such as lead zirconate titanate, barium strontium titanate and alumina, which were fabricated using the sol–gel method in the last decade [38–43]. Their crystallization temperatures were decreased with the seeding. Surface of the seed nanocrystallites was considered to promote crystal growth. Accordingly, the presence of seed crystalline particles in the homogeneous precipitation also may increase crystallinity of ITO particles obtained from precursor particles produced with the homogeneous precipitation. If nuclei of precursor particles are generated in a reaction of raw chemicals in the presence of seed crystalline particles, the nuclei are deposited preferably on the seed crystalline particle surfaces. This means that shape of the seed crystalline particles is reflected by final ITO particles, which indicates that the seeding can vary the shape of the final ITO crystalline particles, and consequently affects electrical properties of ITO films composed of the ITO crystalline particles.

The aim of the present work is to propose a method for fabricating ITO crystalline particles from precursor particles synthesized using a combination of the homogeneous precipitation method and the seeding. Both advantages of the two processes are expected to be reflected for the fabricated particles. Consequently, ITO crystalline particles fabricated utilizing the combination may have identical properties and high crystallinity, and exert dominant electrical properties. Then, electrical conductivity of the ITO crystallites was also studied in the present work.

2. Materials and methods

2.1. Materials

The reactants to produce the seed nanoparticles were indium (III) chloride tetrahydrate ($InCl_3{\cdot}4H_2O$) (>99.95%), tin (IV) chloride pentahydrate ($SnCl_4{\cdot}5H_2O$) (>98.0%) and sodium hydroxide solution (NaOH) (1 M). To fabricate ITO nanoparticles, $InCl_3{\cdot}4H_2O$, $SnCl_4{\cdot}5H_2O$ and urea (>99.0%) were used as an indium source, a tin source and a precipitation-inducer to produce an indium compound and a tin compound, respectively. All chemicals were purchased from Kanto Chemical Co., Inc., and used as received. Water that was ion-exchanged and distilled with Shimadzu SWAC-500 was used in all preparations. The water was deaerated by N_2 gas-bubbling before use in all experiments.

2.2. Methods

2.2.1. Preparation

A colloid solution of seed nanoparticles was synthesized using a coprecipitation process with indium ions, tin ions and a base. An aqueous solution of NaOH was added to an aqueous solution of $InCl_3$ and $SnCl_4$ with vigorous stirring at room temperature (ca. 25 °C). The reaction time was 8 h. The initial In/Sn and NaOH concentrations were 0.009 M/0.001 M and 0.035 M, respectively. The seed nanoparticles were washed by repeated centrifugation, supernatant removal via decantation, water addition and sonication. This procedure was repeated three times. To obtain a concentrated seed nanoparticle colloid solution, the amount of added water was reduced by 1/10, which resulted in concentrations of 0.09 M In and 0.01 M Sn in the final colloid solution.

Precursor particles for ITO were fabricated using the homogeneous precipitation method. The seed nanoparticle colloid solution and a urea aqueous solution were added to a freshly prepared aqueous solution of $InCl_3$ and $SnCl_4$ at room temperature. The mixture was stirred at 80 °C for 8 h. The initial concentrations were 0.00018 M/0.00002 M for In/Sn derived from the seed solution, 0.09 M/0.01 M for In/Sn derived from the freshly prepared solution and 1.55 M for urea, which resulted in a seed content of 2 wt% with respect to the final ITO. The particles in the mixture were washed by repeated centrifugation, supernatant removal via decantation, water addition and sonication. This procedure was repeated three times. To obtain ITO particle powder, the residue at the bottom of the centrifuge tube after the supernatant removal via decantation was dried in vacuo at room temperature to form a powder, which was subsequently annealed in air at 500 °C for 2 h (s-ITO). For comparison, two other types of ITO particles were fabricated from precursor particles. One precursor was particles fabricated using the homogeneous precipitation method without the seed nanoparticles. The other one was the seed nanoparticles in the seed nanoparticle colloid solution. The ITO particle powders (n-ITO and c-ITO, respectively) were obtained from the above-mentioned as-prepared precursor particles, using the identical procedure as that for the ITO that was fabricated with the homogeneous precipitation method.

2.2.2. Characterization

The particles were characterized using transmittance electron microscopy (TEM), scanning electron microscopy (SEM) and X-ray diffractometry (XRD). The TEM was performed using a JEOL JEM-2000FX II microscope at 200 kV. The TEM samples were prepared by dropping and evaporating the particle suspensions onto a colloid-coated copper grid. The SEM was performed using a Hitachi S-4300 microscope at 15 kV. The XRD patterns of the particle powder samples were obtained with a Rigaku Ultima IV X-ray diffractometer at 40 kV and 30 mA with CuKα radiation (λ: 0.154056 nm).

The volume resistivities of the particle powders were measured using a 4-pin probe to determine the electrical resistivity of the particles. Because ITO reduction is a conventionally performed procedure to make the ITO electro-conductive, the reduction procedure was also performed in the present work. The powder was reduced by annealing in H_2/N_2 gas prior to the measurement. The measurements were performed while applying pressure to 2 g of the powder sample in a pressing die set with a diameter of 2.5 cm in the range of 0–300 kg-f/cm^2 using a Mitsubishi Chemical Analytech MCP-T610 resistivity meter.

3. Results and discussion

3.1. Morphology of seed nanoparticles

The inset of Fig. 1 shows a TEM image of the seed nanoparticles. The particle shape was a rectangular parallelepiped, and the particles had an average longitudinal size of 62.2 ± 21.6 nm and a lateral size of 26.2 ± 9.9 nm. Fig. 1 shows an XRD pattern of the seed particles. Several peaks were clearly detected at 22.4°, 31.8°, 39.2°, 51.4°, 56.7°, 66.5°, 71.1° and 75.7°, which correspond to *d*-values of 0.397,

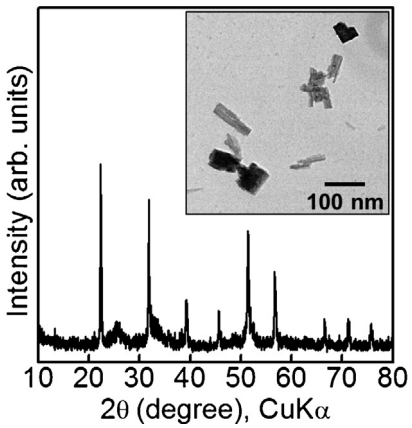

Fig. 1. XRD pattern of the seed particles. The inset shows their TEM image.

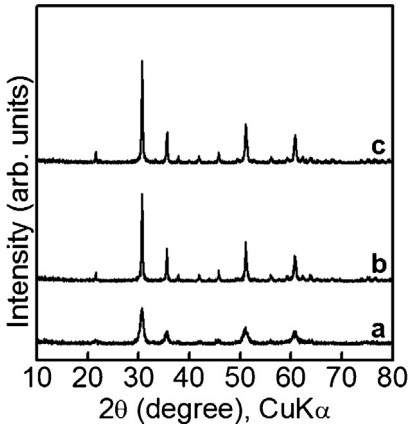

Fig. 3. XRD patterns of (a) c-ITO, (b) n-ITO and (c) s-ITO particles.

0.281, 0.230, 0.178, 0.162, 0.141, 0.132 and 0.126 nm, respectively. These *d*-values were assigned to the (200), (220), (222), (420), (422), (440), (442) and (620) phases of cubic $In(OH)_3$ according to reference [27] and the standard data (ICSD 01-076-146). No other peak was detected, which indicates that Sn^{4+} was doped into the seeds. Application of Scherrer equation to the XRD line broadening of the 22.4° peak provided a crystal size of 37.2 nm. The crystal size was between the longitudinal and lateral sizes. Because the crystal size is calculated in the Scherrer equation assuming that the crystal is spherical, the crystal size obtained in the present work was considered to correspond to the estimated particle size based on the TEM observation. This similarity indicates that the single crystals of $In(OH)_3$ formed the rectangular parallelepiped.

3.2. Morphology of ITO particles

Fig. 2(a1) and (a2) shows an SEM image of the c-ITO particles. The particle shape was quasi-cubic, and the particles had an average size of 57.4 ± 13.5 nm. The quasi-cubic particles formed irregular-shaped agglomerates. Fig. 3(a) shows their XRD pattern. Several peaks were mainly detected at 30.6°, 35.6°, 51.1° and 60.9°, which correspond to *d*-values of 0.292, 0.252, 0.179 and 0.152 nm, respectively. These *d*-values were assigned to the (222), (400), (440) and (622) phases of cubic ITO according to references [24,28] and the standard data (ICSD 01-089-4597). Their crystal size was calculated as 18.5 nm by applying Scherrer equation to the XRD line broadening of the 30.6° peak. The average particle size was larger than the crystal size. Accordingly, the ITO particles were polycrystallites of cubic ITO.

Fig. 2(b1)–(b3) shows an SEM image of the n-ITO particles, in which no seed crystallites were contained. Two types of particle shapes were observed: rectangular parallelepiped (Fig. 2(b2)) and quasi-cubic (Fig. 2(b3)). The particles with the rectangular parallelepiped structure had average sizes of 313 ± 127 nm for the longitudinal direction and 65.7 ± 15.7 nm for the lateral direction, and the quasi-cubic had average sizes of 247 ± 99 nm. Fig. 3(b) shows their XRD pattern. The peaks that were assigned to the (211), (222), (400), (134), (440) and (622) phases of cubic ITO were detected at 21.6°, 30.6°, 35.5°, 45.7°, 51.1° and 60.7°, respectively. Their crystal size was calculated as 34.2 nm from the XRD line broadening of the 30.6° peak. The particle sizes that were obtained in the TEM observation were larger than the crystal size, and no particles with size close to the crystal size were observed. Accordingly, most particles were polycrystallites of cubic ITO. In

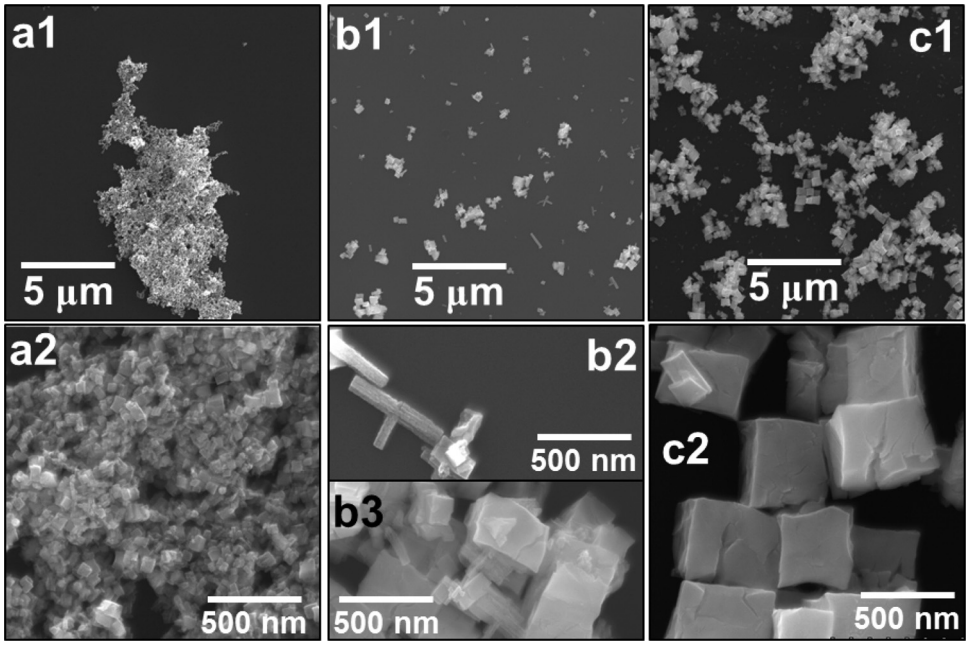

Fig. 2. SEM images of (a) c-ITO, (b) n-ITO and (c) s-ITO nanoparticles with various magnifications.

addition, the two following points should be noted for the XRD. First, the XRD peaks had larger intensities than the ITO particles that were produced using the coprecipitation method, which implies that ITO produced with the homogeneous method has higher crystallinity than that with the coprecipitation method. Accordingly, the homogeneous method is more suitable than the coprecipitation method from the production viewpoint of ITO particles with high crystallinity. Second, the homogeneous method produced larger particle sizes than the coprecipitation method. The homogeneous precipitation method has a smaller reaction rate than the coprecipitation method, which generates a smaller amount of ITO nuclei at an early reaction stage; then, the generated nuclei grow to become the final particles. As a result, larger particles were produced in the homogeneous precipitation method.

Fig. 2(c1) and (c2) shows an SEM image of the s-ITO particles, in which the seed crystallites were contained. Most particles were quasi-cubic. Their average particle size was 438 ± 88 nm, which is larger than that for the ITO with no seed crystallites (n-ITO). The addition of seed nanocrystallites was considered to provide deposition points of the generated ITO nuclei, which promoted the growth of the ITO particles. Fig. 3(c) shows their XRD pattern. Similar to that for the other ITOs in Fig. 3(a) and (b), the peaks were detected at 21.6°, 30.6°, 35.6°, 45.7°, 51.1° and 60.8°, which were assigned to the (2 1 1), (2 2 2), (4 0 0), (1 3 4), (4 4 0) and (6 2 2) phases of cubic ITO, respectively. Their calculated crystal size based on the XRD line broadening of the 30.6° peak was 31.2 nm. Similar to the ITO with no seeds, most particles were polycrystallites of cubic ITO because the particle size was larger than the crystal size. The XRD peak intensities were slightly larger than those of ITO with no seeds. Accordingly, the addition of seed nanocrystallites promotes the particle growth and increases their crystallinity, although its effect is small.

In a preliminary experiment, pH of 1.55 M for urea reached ca. 7 with heating at 80 °C for 8 h. Solubility products of $In(OH)_3$ and $Sn(OH)_4$ are 6.3×10^{-34} M^4 and 1×10^{-56} M^5, respectively [44]. Calculation using the pH and the solubility products provided concentrations of 6.3×10^{-13} M for In ions and 1×10^{-28} M for Sn ions at the pH 7. Accordingly, almost the In ions and the Sn ions were precipitated due to the initial concentrations of 0.09 M $InCl_3$ and 0.01 M $SnCl_4$. Taking into account of the initial concentrations and the solubility products, the In ions and the Sn ions should have been precipitated at pH of 3.3 and 0.5 in the present work, respectively. Therefore, the Sn ions were considered to be precipitated earlier; it was hard to conclude simultaneous precipitation of these ions because of the difference in solubility products, which may have spoiled homogeneity of ITO particles. Electrical properties of ITO particles are possibly related to their homogeneity, which is discussed in the following section.

3.3. Electrical properties of ITO particles

Plot (a) in Fig. 4 shows the dependence of the volume resistivity on pressure for c-ITO particles. The volume resistivity monotonically decreased from 1.48 to 0.141 Ω cm with an increase in pressure from 2 to 300 kg-f/cm^2. In a preliminary experiment, powder sample became thin with applying pressure to the powder sample, the powder was densely packed under the pressure. Since packing density of powder sample is an important factor to govern its electric properties, the volume resistivity was discussed using the packing density, as follows. A thickness of the powder sample was measured after each application of pressure, and a bulk density of the powder sample was calculated from the thickness and the pellet diameter of 2.5 cm. Packing density of the powder sample was calculated from the bulk density and the density of ITO (ca. 7.12 g/cm^3). The plot (a) in Fig. 4 was re-plotted to the volume resistivity versus the packing density, as shown in plot (a) in Fig. 5.

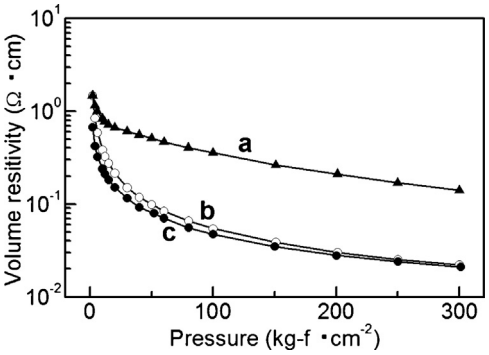

Fig. 4. Volume resistivities of (a) c-ITO, (b) n-ITO and (c) s-ITO particle powders as a function of the applied pressure.

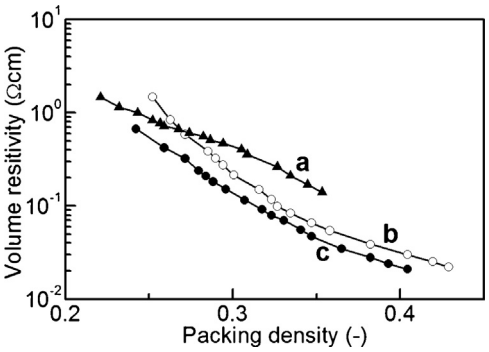

Fig. 5. Volume resistivities of (a) c-ITO, (b) n-ITO and (c) s-ITO particle powders as a function of the packing density.

The monotonic decrease in volume resistivity took place with the increase in packing density from 0.221 to 0.353. The application of pressure to the particle powder provided the increase in packing density of particle powder, so that the particles made contact with one another. As a result, their conductivity increased, i.e., the volume resistivity decreased.

Plot (b) in Fig. 4 shows the volume resistivity of the n-ITO particles as a function of pressure. The volume resistivity also monotonically decreased with increasing pressure. Plot (b) in Fig. 5 shows the volume resistivity of the n-ITO particles versus the packing density. The volume resistivity decreased from 1.48 to 0.0223 Ω cm with an increase in packing density from 0.252 to 0.428. In the range smaller than ca. 0.26, the resistivities were larger than those for the c-ITO particles. The c-ITO particles could form agglomerates because of the size smaller than that of the n-ITO particles, which secured routes passing electric current in the pellet. In contrast, over the packing density of ca. 0.26, the volume resistivities were smaller than those for the c-ITO nanoparticles. Contact among the particles that formed angular structures such as rectangular parallelepiped and quasi-cubic began to become strong at the larger packing densities, which decreased the contact resistivity among the particles. Consequently, the volume resistivity was decreased.

Plot (c) in Fig. 4 shows the volume resistivity of the s-ITO particles as a function of pressure. The volume resistivity also decreased with an increase in pressure. The volume resistivity of the s-ITO particles as a function of the packing density is shown in Plot (b) in Fig. 5. The volume resistivity decreased from 0.675 to 0.0211 Ω cm with an increase in packing density from 0.242 to 0.404. The volume resistivity was smaller than that of the n-ITO particles in the range of all the packing densities. According to the TEM observation (Fig. 2(c)), most particles were quasi-cubic, and their size was nearly mono-dispersed. The same shape and the mono-dispersion

probably made the particles have stronger contact than the n-ITO particles, which decreased the volume resistivity.

Volume resistivities of ITO films are in the range of 10^{-3}–10^{-4} Ω cm, which have been reported by several researchers [4,5,11–13]. The volume resistivities obtained in the present work were larger than the reported volume resistivities. The large volume resistivities may have been related to the spoiled homogeneity of ITO particles, which was implied in the previous section. Accordingly, the homogeneity is required to be investigated with analysis techniques such as X-ray photoelectron spectroscopy and energy dispersive X-ray spectrometry that can give distribution of atoms and bonds for better understanding of a mechanism on the electrical properties and for improving them, and is in progress.

4. Conclusions

Colloidal solutions of precursor particles for ITO were prepared using a homogeneous precipitation method, where the reaction of In^{3+}, Sn^{4+} and urea was initiated by heating at 80 °C in the presence of seed nanoparticles, which were produced using the co-precipitation method with $InCl_3$, $SnCl_4$ and NaOH. The as-prepared precursor particles were transformed into a powder of ITO by annealing in air at 500 °C. The c-ITO particles formed the irregular-shaped agglomerates. In contrast, the n-ITO particles formed angular particles with rectangular parallelepiped and quasi-cubic shapes. The seeding produced only the quasi-cubic particles and increased the particle size. According to the conductivity measurements, the volume resistivity of the s-ITO particle powder was in the range of 0.675–0.0211 Ω cm at packing densities of 0.242–0.404, which was the smallest value among the examined ITO particles; the combination of the homogeneous precipitation method and seeding technique provided production of large ITO particles with regular size and shape. This method allowed us to make the particles strongly in contact with one another. Consequently, the small volume resistivity was recorded for the s-ITO particle powder.

Acknowledgments

This work was partially supported by the Mitsubishi Materials Corporation (Ref. No.: 24-329).

References

[1] M. Mahajeri, A. Schneider, M. Baum, T. Rechtenwald, M. Voigt, M. Schmidt and W. Peukert, Thin Solid Films, 520, 5741–5745 (2012).
[2] C.E.J. Cordonier, A. Nakamura, K. Shimada and A. Fujishima, Thin Solid Films, 520, 5867–5876 (2012).
[3] I.Y.Y. Bu, Ceram. Int., 40, 3445–3451 (2014).
[4] K. Shinoda, T. Nakajima and T. Tsuchiya, Appl. Surf. Sci., 292, 1052–1058 (2014).
[5] M. Kiristi, A. Gulec, F. Bozduman, L. Oksuz, A.U. Oksuz and A. Hala, Thin Solid Films, 567, 32–37 (2014).
[6] T. Olav, L. Sunde, M.-A. Einarsrud and T. Grande, Thin Solid Films, 573, 48–55 (2014).
[7] Z. Xu, P. Chen, Z. Wu, F. Xu, G. Yang, B. Liu, C. Tan, L. Zhang, R. Zhang and Y. Zheng, Mater. Sci. Semiconduct. Process., 26, 588–592 (2014).
[8] V.S. Vaishnav, S.G. Patel and J.N. Panchal, Sens. Actuators B, 206, 381–388 (2015).
[9] M. Tului, A. Bellucci, S. Bellini, A. Albolino and G. Migliozzi, Thin Solid Films, 520, 4041–4045 (2012).
[10] H. Lei, M. Wang, Y. Hoshi, T. Uchida, S. Kobayashi and Y. Sawada, Appl. Surf. Sci., 285P, 389–394 (2013).
[11] A. Sytchkova, D. Zola, L.R. Bailey, B. Mackenzie, G. Proudfoot, M. Tian and A. Ulyashin, Mater. Sci. Eng. B, 178, 586–592 (2013).
[12] J.M. Gaskell and D.W. Sheel, Thin Solid Films, 520, 4110–4113 (2012).
[13] P.D. Szkutnik, H. Roussel, V. Lahootun, X. Mescot, F. Weiss and C. Jiménez, J. Alloys Compd., 603, 268–273 (2014).
[14] S. Marikkannu, M. Kashif, N. Sethupathy, V.S. Vidhya, S. Piraman, A. Ayeshamariam, M. Bououdina, N.M. Ahmed and M. Jayachandran, Mater. Sci. Semiconduct. Process., 27, 562–568 (2014).
[15] V. Brinzari, I. Damaskin, L. Trakhtenberg, B.K. Cho and G. Korotcenkov, Thin Solid Films, 552, 225–231 (2014).
[16] M.A.H. Khondoker, S.Y. Yang, S.C. Mun and J. Kim, Synth. Met., 162, 1972–1976 (2012).
[17] A. Yabuki, K. Okumura and I.W. Fathona, Chem. Eng. J., 252, 275–280 (2014).
[18] K. Hoshino, R. Nakajima and M. Okuma, Appl. Surf. Sci., 313, 569–576 (2014).
[19] M.-K. Jeon and M. Kang, Mater. Lett., 62, 676–682 (2008).
[20] R. Sarhaddi, N. Shahtahmasebi, M.R. Rokn-Abadi and M.M. Bagheri-Mohagheghi, Physica E, 43, 452–457 (2010).
[21] X. Li, X. Xu, X. Yin, C. Li and J. Zhang, Particuology, 9, 471–474 (2011).
[22] L. Kőrösi, A. Scarpellini, P. Petrik, S. Papp and I. Dékány, Appl. Surf. Sci., 320, 725–731 (2014).
[23] A. Ayeshamariam, M. Kashif, M. Bououdina, U. Hashim, M. Jayachandran and M.E. Ali, Ceram. Int., 40, 1321–1328 (2014).
[24] S. Li, X. Qiao, J. Chen, H. Wang, F. Jia and X. Qiu, J. Cryst. Growth, 289, 151–156 (2006).
[25] J. Li, H. Fu, L. Fu and J. Hao, Environ. Sci. Technol., 40, 6455–6459 (2006).
[26] J.T. McCue and J.Y. Ying, Chem. Mater., 19, 1009–1015 (2007).
[27] B. Xu, B. Yang, Y. Guo, D. Liu, Q. Yu and S. Wei, J. Alloys Compd., 509, 4538–4542 (2011).
[28] H.-C. Lu, J.-W. Mao and Y.-C. Chiang, Surf. Coat. Technol., 231, 526–530 (2013).
[29] A. Soliemana, M.K. Zayeda, S.N. Alamri, N. Al-Dahoudi and M.A. Aegerter, Mater. Chem. Phys., 134, 127–132 (2012).
[30] L. Diamandescu, D. Tarabasanu-Mihaila, M. Fedea, M. Enculescu, V.S. Teodorescu, S. Constantinescu, T. Popescu, C. Bartha and Zs. Pap, Mater. Chem. Phys., 143, 1540–1549 (2014).
[31] Y.-C. Chang, J. Alloys Compd., 615, 538–541 (2014).
[32] M.T.S. Tavares, L.X. Lovisa, V.D. Araújo, E. Longo, M.S. Li, R.M. Nascimento, C.A. Paskocimas, M.R.D. Bomio and F.V. Motta, Mater. Sci. Semiconduct. Process., 27, 1036–1041 (2014).
[33] P. Wan, W. Yang, X. Wang, J. Hu and H. Zhang, Sens. Actuators B, 214, 36–42 (2015).
[34] P.-Y. Song and W.-D. Zhang, Mater. Res. Bull., 53, 177–184 (2014).
[35] X. Tao, Y. Zhao, L. Sun and S. Zhou, Mater. Chem. Phys., 149–150, 275–281 (2015).
[36] S. Nagashima, T. Yoshida and A. Kato, Mater. Lett., 19, 171–176 (1994).
[37] H. Xu and A. Yu, Mater. Lett., 61, 4043–4045 (2007).
[38] T. Tanase, A. Nishikata, Y. Iizuka, Y. Kobayashi, M. Konno and T. Miwa, J. Ceram. Soc. Jpn., 110, 911–915 (2002).
[39] T. Tanase, Y. Kobayashi, T. Miwa and M. Konno, Mater. Res. Soc. Symp. Proc., 784, C3.32.1–C3.32.6 (2004).
[40] T. Tanase, Y. Kobayashi, T. Nabatame, T. Miwa and M. Konno, Thin Solid Films, 471, 71–75 (2005).
[41] Y. Kobayashi, Y. Iizuka, T. Tanase and M. Konno, J. Sol-Gel Sci. Technol., 33, 315–321 (2005).
[42] K. Inoue, M. Hama, Y. Kobayashi, Y. Yasuda and T. Morita, ISRN Ceram., 2013, 317830 (2013).
[43] Y. Kobayashi, Y. Mabuchi, M. Hama, K. Inoue, Y. Yasuda and T. Morita, J. Asian Ceram. Soc., 3, 139–143 (2015).
[44] in Lange's Handbook of ChemistryJ.E. Dean, 12th ed., McGraw-Hill, New York (1978).